Available online at www.sciencedirect.com
SCIENCE DIRECT
Journal of Power Sources 155 (2006) 353–357
JOURNAL OF POWER SOURCES
www.elsevier.com/locate/jpowsour

Short communication

Solid oxide fuel cells operated by internal partial oxidation reforming of *iso*-octane

Zhongliang Zhan, Scott A. Barnett *

Department of Materials Science and Engineering, Cook Hall 2036, 2220 N. Campus Drive, Northwestern University, Evanston, IL 60208, USA

Received 25 March 2005; received in revised form 21 April 2005; accepted 21 April 2005
Available online 22 June 2005

Abstract

Two types of solid oxide fuel cells (SOFCs), with thin $Ce_{0.85}Sm_{0.15}O_{1.925}$ (SDC) or 8 mol% Y_2O_3-stabilized ZrO_2 (YSZ) electrolytes, were fabricated and tested with *iso*-octane/air fuel mixtures. An additional Ru–CeO_2 catalyst layer, placed between the fuel stream and the anode, was needed to obtain a stable output power density without anode coking. Thermodynamic analysis and catalysis experiments showed that H_2 and CO were primary reaction products at ≈750 °C, but that these decreased and H_2O and CO_2 increased as the operating temperature dropped below ≈600 °C. Power densities for YSZ cells were 0.7 W cm^{-2} at 0.7 V and 790 °C, and for SDC cells were 0.6 W cm^{-2} at 0.6 V and 590 °C. Limiting current behavior was observed due to the relatively low (≈20%) H_2 content in the reformed fuel.

Keywords: Solid oxide fuel cells; Catalyst; Hydrocarbons; *Iso*-octane; Partial oxidation

1. Introduction

There has been recent interest in the use of solid oxide fuel cells (SOFCs) in applications for portable power generation [1–3] and auxiliary power units (APUs) for transportation [4]. These applications utilize fuels, such as propane, gasoline, diesel, and kerosene, which have two main advantages compared with the hydrogen commonly used in fuel cells. First, the refining and distribution infrastructure for these fuels is well established. Second, energy densities are considerably larger, e.g. 34 MJ l^{-1} for gasoline, than even liquefied or highly compressed (800 bar) hydrogen (10 MJ l^{-1}). In order to work with fuel cells, such fuels are typically reformed to hydrogen-rich mixtures using partial oxidation reforming in a separate reformer [5] or elsewhere within the stack [6]. Especially for smaller-scale applications, it would be useful to do internal reforming on the SOFCs, in order to reduce power plant size, weight, and complexity, and to provide a heat source within the stack.

There have been a number of recent examples of SOFCs operating by direct internal partial oxidation (POx) reforming of hydrocarbon fuels. Hibino and co-workers have reported the use of internal POx reforming of various fuels in single-chamber SOFCs, resulting e.g. in a power density of 0.24 W cm^{-2} at 550 °C with propane/air mixtures [7]. Internal POx of butane has been reported in microtubular SOFCs [2,3], yielding a power density of 0.1 W cm^{-2} at 700 °C. Recently, we reported an output power density of 0.70 W cm^{-2} at 790 °C or 0.38 W cm^{-2} at 690 °C with propane–air mixtures in conventional dual-chamber YSZ electrolyte anode-supported fuel cells [8]. Ru–CeO_2 layers have been added to SOFCs to catalyze propane partial oxidation at temperatures down to ≈400 °C [9], helping to enable thermally self-sustaining single-chamber SOFC stacks that yielded a power output of ∼350 mW (active area = 1.42 cm^2) at 500–600 °C [10]. However, internal partial oxidation of liquid hydrocarbon fuels, e.g. gasoline and diesel, has not been demonstrated.

In this paper, we describe results on the operation of SOFCs on mixtures of air and *iso*-octane, chosen as a typical liquid hydrocarbon fuel. YSZ electrolyte cells with Ni–YSZ

* Corresponding author. Tel.: +1 847 491 2447; fax: +1 847 491 7820.
E-mail address: s-barnett@northwestern.edu (S.A. Barnett).

0378-7753/$ – see front matter © 2005 Elsevier B.V. All rights reserved.
doi:10.1016/j.jpowsour.2005.04.015

anode supports were tested from 600–800 °C, and SDC electrolyte cells with Ni–SDC anode supports were tested at 400–600 °C. A Ru–CeO_2 catalyst layer placed against the anode surface was found to be critical to obtaining stable operation without coking.

2. Experimental

The SOFCs were prepared using standard ceramic processing procedures as described elsewhere [11]. Briefly, the SDC-electrolyte SOFCs had 0.6 mm-thick Ni–SDC anode supports with 40 wt.% $Ce_{0.85}Sm_{0.15}O_{1.925}$ (SDC) (18 $m^2\,g^{-1}$, Nextech) and 60 wt.% NiO (4 $m^2\,g^{-1}$, J.T. Baker). After bisque firing at 800 °C for 4 h, a 15 μm-thick NiO–SDC anode active layer and a 10 μm-thick thin SDC electrolyte layer were deposited on the NiO–SDC support from an ethanol-based colloidal solution, using a process similar to that described by Jiang and Virkar [12]. The support and layers were then co-fired at 1400 °C for 6 h. Cathode active layers consisted of $La_{0.6}Sr_{0.4}Co_{0.2}Fe_{0.8}O_3$ (LSCF) (4 $m^2\,g^{-1}$, Praxair) mixed with 30 wt.% SDC, fired at 1100 °C for 4 h. A second layer of pure LSCF was applied using conditions similar to those above. For YSZ (8 mol% Y_2O_3–stabilized ZrO_2)-electrolyte SOFCs, the anode supports had 0.6 mm-thick Ni–YSZ anode supports with 50 wt.% ZrYO (YSZ) (7 $m^2\,g^{-1}$, Tosoh) and 50 wt.% NiO (4 $m^2\,g^{-1}$, J.T. Baker). After bisque firing at 1100 °C for 4 h, a 15 μm-thick NiO–YSZ anode active layer and a 7 μm-thick thin YSZ electrolyte layer were then colloidally deposited on the NiO–YSZ support, and co-fired at 1400 °C for 6 h. LSCF–$Ce_{0.9}Gd_{0.1}O_{1.95}$ (GDC, 180 $m^2\,g^{-1}$, Nextech) cathode layers were applied and fired at 900 °C for 4 h, in order to minimize zirconate formation [13]. Then a second layer of pure LSCF slurry was applied and fired at 900 °C for 4 h. The final fuel cells were 1.3–1.5 cm in diameter, with anode thickness of 0.6 mm, electrolyte thickness of 7–10 μm, and cathode thickness of 20–30 μm. Estimated anode porosity was ≈35%, and cathode porosity was ≈30%.

The catalysts were prepared on 0.5 mm-thick discs of partially stabilized zirconia (PSZ, 7 $m^2\,g^{-1}$, Tosoh). The PSZ was mixed with starch pore former to introduce substantial porosity, pressed, and fired at 1400 °C for 4 h. RuO_2 (45–70 $m^2\,g^{-1}$, Aldrich) and CeO_2 (15 $m^2\,g^{-1}$, Inframat) powders in a 1:10 weight ratio were combined in a colloidal suspension with ethanol as the solvent, deposited on both sides of the PSZ, and fired at 900 °C for 4 h to form 10–20 μm-thick catalyst layers.

Single SOFCs were tested in a tube furnace at setpoint temperatures from 400 to 800 °C. In many cases the "catalyst" discs were placed directly against the SOFC anode. Since the thick insulating catalyst layer prevents current collection through the anode, current was collected at the side of the anode. Ambient air was maintained on the cathode side. After reducing the anode Ni and catalyst Ru and testing in humidified hydrogen, testing was done in *iso*-octane/air mixtures obtained by flowing 100 sccm air through a bubbler containing *iso*-octane at 296 K (yielding ≈ 6.2% *iso*-octane, i.e. an O_2 to C_8H_{18} ratio χ of 3.2). Separate catalysis experiments were carried out in a similar measurement setup where the catalyst was placed against a dense YSZ piece (instead of a fuel cell) and the fuel exhaust gas was analyzed using a Transpector 2® Gas Analysis System (Inficon L100). Note that a 21% O_2–79% Ar mixture was used in place of "air" in order to avoid the interference between N_2 and CO at mass 28 in mass spectrometer measurements. The composition $\chi = 3.2$ was chosen to be outside the flammability range (1–6%) but near the ratio $\chi = 4$ for partial oxidation. The *I–V* curves were obtained using an IM6 Electrochemical Workstation (ZAHNER, Germany). We have calibrated the cell temperature by observing changes in the ohmic portion of electrochemical impedance spectra upon switching the fuel from hydrogen to octane/air. That is, the temperature was determined via the temperature dependence of the electrolyte resistance [9]. The calibration was done using YSZ-electrolyte SOFCs, since the electrolyte resistance measurement is complicated by electronic conductivity in the SDC-electrolyte cells. The measurements indicated that the actual cell temperature was ≈40 °C higher than the furnace temperature. Cell temperature values in the results presented below include this correction.

3. Results and discussion

Attempts to operate the SOFCs on *iso*-octane/air mixtures, without a catalyst layer, were unsuccessful. A life test was run with a SDC cell at 590 °C on *iso*-octane carried by 100 sccm air (Fig. 1). The cell performance was initially good, i.e. a voltage of 0.6 V at 0.8 A cm^{-2}, but the voltage decreased by ≈20% over 20 h. A life test with a YSZ cell at 790 °C with the same fuel yielded a similar result, with the terminal voltage at 0.6 A cm^{-2} decreasing gradually. For both types of cells, subsequent observation of the anodes showed severe coke buildup, presumably explaining the degradation. In order to

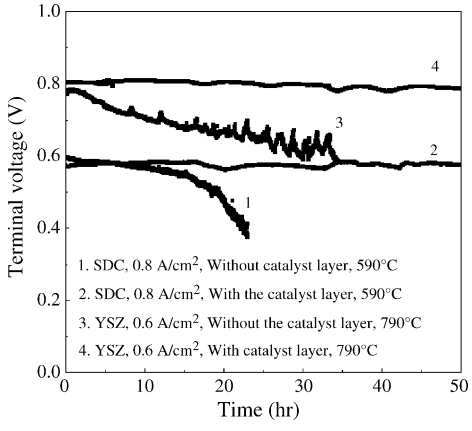

Fig. 1. Cell performance vs. time for YSZ or SDC electrolyte SOFCs, tested with or without catalyst layers, during operation on 6% *iso*-octane–94% air at 100 sccm.

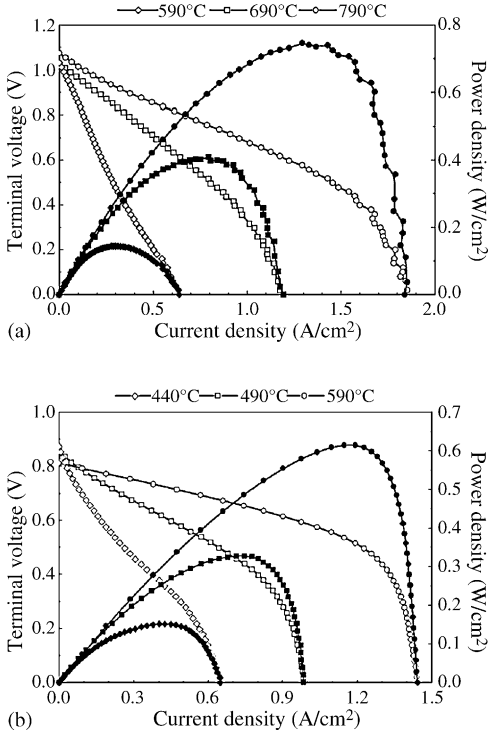

Fig. 2. Voltage and power density vs. current density for the cells: (a) NiO–YSZ |YSZ| LSCF–GDC, LSCF, or (b) Ni–SDC |SDC| LSCF–SDC, LSCF, tested with 6% *iso*-octane–94% air at 100 sccm in the anode and ambient air in the cathode. Both tests were done with a Ru–CeO_2 catalyst layer.

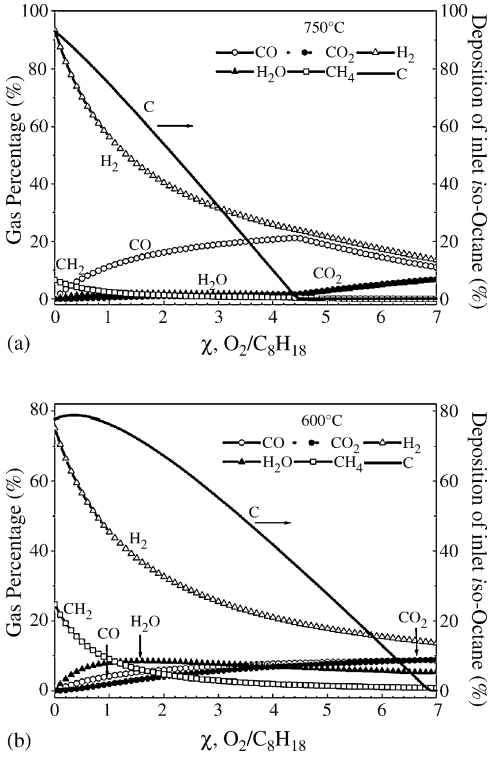

Fig. 3. Calculated equilibrium gaseous product composition, and fraction of inlet carbon deposited as solid carbon, as a function of oxygen-to-*iso*-octane ratio χ at: (a) 750 °C and (b) 600 °C. The starting fuel consisted of *iso*-octane, oxygen and argon, with Ar to O_2 ratio fixed at 79/21.

improve stability, cells were tested with Ru–CeO_2 catalyst layers placed in contact with the anode support. With the addition of the catalyst layer between the fuel stream and the anode, both SDC and YSZ cells became quite stable (Fig. 1). No C was detected on either the anode or the catalyst after stable operation with the catalyst layer.

The cell performance with *iso*-octane/air with the catalyst layer is shown for YSZ cells (Fig. 2a) and SDC cells (Fig. 2b). Each data point was acquired after a hold time of 10 ms. Measured OCV values for YSZ cells ranged from 1.03 V at 600 °C to 1.10 V at 800 °C, in good agreement with the values from 1.05 to 1.11 V predicted using the effective oxygen partial pressure of the equilibrated fuel (see the thermodynamic calculation below). Measured OCV values for SDC cells were much lower, 0.8–0.9 V. This behavior is typical for mixed conducting SDC electrolytes [14–16], and is explained by an electronic leakage current in the thin electrolyte [17,18]. Power values with *iso*-octane/air increased with increasing T, but limiting current densities of ≈1–2 A cm^{-2} were observed at higher T for both types of cells, limiting the maximum power values. Limiting currents were much larger (>3.5 A cm^{-2}) when these cells were run with hydrogen fuel. Impedance spectroscopy measurements at open circuit from these cells yielded typical area-specific resistance values of 0.07 Ω cm^2 for the electrolyte and 0.5 Ω cm^2 for the electrodes in the YSZ cells at 790 °C; versus 0.06 Ω cm^2 for the electrolyte and 0.15 Ω cm^2 for the electrodes in the SDC cells at 590 °C.

In order to understand the above results, we used a standard free energy minimization calculation [8] to predict the equilibrium reaction product composition versus the oxygen-to-*iso*-octane ratio χ for typical temperatures of 750 °C (Fig. 3a), and 600 °C (Fig. 3b). The results show that coking was expected at both temperatures for the value $\chi = 3.2$ used in the experiments. Indeed, C was eliminated only for $\chi \geq 4.5$ at 750 °C, and for $\chi \geq 6.9$ at 600 °C. Thus, the observed coking of unprotected Ni anodes was expected. On the other hand, the non-coking of Ru-based catalysts can only be explained by the well-known resistance of Ru to coking [19].

Fig. 3 also shows that all gas-phase products decreased with increasing χ, as they became increasingly diluted by the inert portion of the air (i.e. Ar in this case). At 750 °C and low χ, the main products are C and H_2. The amount of C decreases and CO increases with increasing χ. For the oxygen-to-*iso*-octane ratio of 3.2 used in the present experiments, H_2 and CO comprise most of the gaseous reaction products at 750 °C, with only slight amounts of H_2O and CO_2 produced. This is good since H_2 and CO are readily utilized by the SOFC. However, the equilibrium fractions of H_2O and CO_2 increase and H_2 and CO decrease with decreasing temperature, as can be seen in Fig. 3. These results suggest that higher operating temperatures will be preferred for applications where high

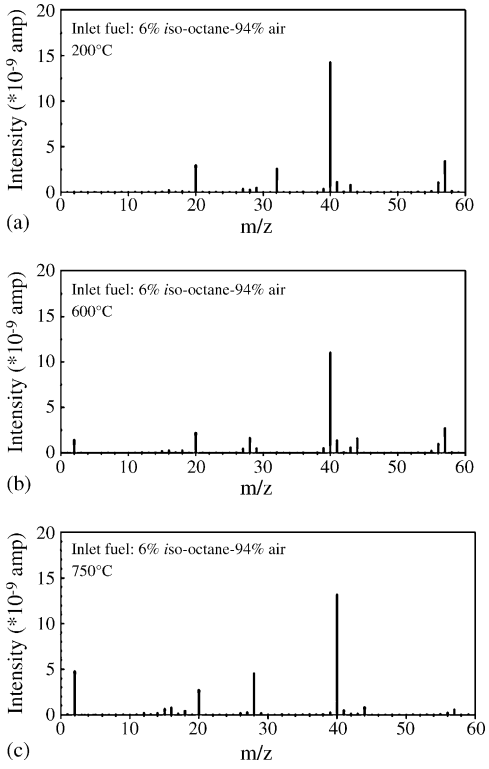

Fig. 4. Typical mass spectra of catalyst reaction products for an input fuel composition of 6% *iso*-octane–94% air at furnace setpoint temperatures of: (a) 200 °C, (b) 600 °C and (c) 750 °C. The peak masses (AMU) were assigned as follows: $H_2 = 2$, $CH_4 = 16$, $H_2O = 18$, $CO = 28$, $O_2 = 32$, $Ar = 40$, $CO_2 = 44$, $C_8H_{18} = 57$.

fuel efficiency is needed, unless highly selective low temperature partial oxidation catalysts can be found.

The catalysis products were measured using a differentially-pumped mass spectrometer, while ramping up the furnace temperature at a rate of 10 °C min^{-1}. Note that H_2O was trapped to avoid poisoning the mass spectrometer. Fig. 4 shows typical mass spectra of catalyst reaction products at three different temperatures, after flowing a 6% *iso*-octane–94% air mixture at 100 sccm over a Ru–CeO_2 catalysis layer. The 200 °C spectrum (Fig. 4a) shows peaks at atomic mass 20 (Ar^{++}), 32 (O_2^+), 40 (Ar^+), and 57 ($C_4H_9^+$ or $C_8H_{18}^{++}$), corresponding to the input gas composition. Other peaks were at or near background levels. Above ≈280 °C, peaks at mass 2 (H_2^+), 28 (CO^+), and 44 (CO_2^+) increased significantly while the O_2^+ and $C_8H_{18}^{++}$ peaks decreased relative to Fig. 4a, as shown for 600 °C (Fig. 4b) and 750 °C (Fig. 4c). A small peak at mass 16 (CH_4^+) was also present. Note that the H_2, CO, and CO_2 peak intensities were comparable at 600 °C, whereas H_2 and CO were predominant at 750 °C, in agreement with Fig. 3. While O_2 was at background levels at both 600 and 750 °C, indicating complete combustion, significant C_8H_{18} appeared to be present at 600 °C. This was probably due to the tendency of *iso*-octane to accumulate in the mass spectrometer gas lines, such that the C_8H_{18} peak was retained longer than expected during the temperature ramp.

In summary, these results suggest that the *iso*-octane fuel was almost completely reformed by the catalyst layer at SOFC operating temperatures, providing a good supply of $H_2 + CO$ and preventing C_8H_{18} cracking at the Ni anode.

Fig. 3 indicates that the catalysis reaction supplied ≈29% H_2 and ≈20% CO at 750 °C or ≈24% H_2 and ≈8% CO at 600 °C to the SOFC anode. The mass spectrometer results in Fig. 4 were consistent with these numbers. These concentrations are low enough to produce substantial concentration polarization in the SOFC characteristics even with low fuel utilization (<30%), as seen in Fig. 2. Similar behavior was reported previously for SOFCs operated on propane–air mixtures, where the H_2 partial pressure in the reformed fuel was low, ≈20% [8,20]. The results suggest that the *iso*-octane/air cell performance can be improved by increasing anode porosity.

4. Summary and conclusions

In summary, we have successfully operated both conventional and reduced-temperature SOFCs by internal partial oxidation of *iso*-octane. The present results suggest that the catalyst layer almost completely reformed the *iso*-octane fuel at SOFC operating temperatures, thereby eliminating Ni anode coking. The key advantages to having the catalyst in direct contact with the cells include: (1) the catalysis and electrochemical reactions are coupled, i.e. electrochemical consumption of CO and H_2, along with the production of CO_2 and H_2O, should help increase the syngas output, (2) electrochemically produced CO_2 and H_2O will result in some endothermic reforming reactions, potentially improving fuel efficiency, and (3) the heat from the partial oxidation reaction will be more effectively distributed throughout the stack.

Acknowledgements

The authors gratefully acknowledge the financial support of the Defense Advanced Research Projects Agency, funded via California Institute of Technology, during the course of this work. The authors thank Dr. Yi Jiang for describing the colloidal “drop coating” technique used for depositing the electrolyte layers, and thank Prof. Sossina Haile and Dr. Zongping Shao for useful discussions.

References

[1] K. Hayashi, O. Yamamoto, H. Minoura, Solid State Ionics 132 (2000) 343–345.
[2] K. Kendall, M. Palin, J. Power Sources 71 (1998) 268–270.
[3] N.M. Sammes, R.J. Boersma, G.A. Tompsett, Solid State Ionics 135 (2000) 487–491.
[4] S. Mukerjee, M.J. Grieve, K. Haltiner, M. Faville, J. Noetzel, K. Keegan, D. Schumann, D. Armstrong, D. England, J. Haller, in: S.C. Singhal, H. Yokokawa (Eds.), Proceedings of the Seventh

International Symposium on Solid Oxide Fuel Cells, The Electrochemical Society, Pennington, 2001.
[5] J. Botti, in: S.C. Singhal, H. Yokokawa (Eds.), Proceedings of the Eighth International Symposium on Solid Oxide Fuel Cells, The Electrochemical Society, Pennington, 2003, pp. 16–30.
[6] R.A. George, A.C. Casanova, S.E. Veyo, Fuel Cell Seminar Abstract (eds Fuel Cell Seminar Committee), Courtesy Associates, Washington, 2002 pp. 977–979.
[7] T. Hibino, A. Hashimoto, T. Inoue, J. Tokuno, S. Yoshida, M. Sano, Science 288 (2000) 2031–2033.
[8] Z. Zhan, J. Liu, S.A. Barnett, Appl. Catal. A: Gen. 262 (2004) 255–259.
[9] Z. Zhan, S.A. Barnett, Solid State Ionics 176 (2005) 871–879.
[10] Z. Shao, S. Haile, J. Ahn, P. Ronney, Z. Zhan, S. Barnett, Nature, in press.
[11] J. Liu, S.A. Barnett, J. Am. Ceram. Soc. 85 (2002) 3096–3098.
[12] Y. Jiang, A.V. Virkar, J. Electrochem. Soc. 148 (7) (2001) A706–A709.
[13] E.P. Murray, M.J. Sever, S.A. Barnett, Solid State Ionics 148 (2002) 27–34.
[14] C.R. Xia, F.L. Chen, M.L. Liu, Electrochem. Solid State Lett. 4 (5) (2001) A52–A54.
[15] C.R. Xia, M.L. Liu, Solid State Ionics 144 (3–4) (2001) 249–255.
[16] R. Doshi, V.L. Richards, J.D. Carter, X.P. Wang, M. Krunmpelt, J. Electrochem. Soc. 146 (1999) 1273–1278.
[17] M. Godickemeier, D. Schneider, L.J. Gauckler, Proceedings of the Fifth European Symposium on SOFCs, European Fuel Cell Group Ltd., Lucerne, Switzerland, Oct 3–7, 1997, pp. 1011–1016.
[18] T. Matsui, T. Kosaka, M. Inaba, A. Mineshige, Z. Ogumi, Solid State Ionics 176 (2005) 663–668.
[19] A. Ashcroft, A. Cheetham, M. Green, P. Vernon, Nature 352 (1991) 225–226.
[20] Z. Zhan, S.A. Barnett, Fuel Cell Seminar Abstracts, Miami Beach, Florida, US, 2003, pp. 808–811.